23rd ABCM International Congress of Mechanical Engineering
December 6-11, 2015, Rio de Janeiro, RJ, Brazil

AEROACOUSTIC INVESTIGATION OF AN AIRFOIL IMMERSED IN A VORTEX WAKE

Bruno Backes
William R. Wolf
University of Campinas - UNICAMP
bbackes@fem.unicamp.br
wolf@fem.unicamp.br

Abstract. *The present work concerns the study of aerodynamic noise generation and propagation from an airfoil immersed in a vortex wake. This investigation is of paramount importance for the design of aerodynamic configurations such as wings and high-lift devices as well as gas turbines and wind turbine blades, fans and propellers. In take-off and landing configurations, vortical structures from slat and wing impinge on the leading edges of wing and flap, respectively. In rotating configurations such as wind turbines, helicopter blades, industrial fans and propellers, the wake generated from the airfoil impinges on its own leading edge. The current research project consists of an investigation of the physical mechanisms of airfoil noise generation due to vortex wakes generated from a cylinder placed upstream of an airfoil. This simplified flow configuration allows a parametric study of noise sources from airfoil leading edges. It must be mentioned that, in this problem, the presence of additional noise sources are also considered in the analysis. For example, one should mention the noise generated from the unsteady loading along the cylinder surface and from the airfoil trailing edge, beyond the noise from quadrupole-type sources present in the aerodynamic wakes from both geometries. The flow compressibility effects, cylinder positioning upstream of the airfoil and the ratio between vortex length and leading edge radius of curvature is investigated. Direct Numerical Simulation (DNS) is the numerical method of choice to simulate the present flows of interest since it captures all the energy scales associated with noise generation and propagation. The aeroacoustic calculations is performed using DNS and the Ffowcs Williams & Hawkings (FWH) acoustic analogy formulation.*

Keywords: *Leading edge noise, Aeroacoustics, Fluid-structure interaction*

1. INTRODUCTION

High-lift devices are important sources of airframe noise. In take-off and landing configurations, vortical structures from slat and wing impinge on the leading edges of wing and flap, respectively. In rotating configurations such as wind turbines, helicopter blades, industrial fans and propellers, the wake generated by the airfoil impinges on its own leading edge. The current paper presents an investigation of the physical mechanisms of leading edge noise generation from a vortex wake impinging on an airfoil. Here, the vortex wake is generated by a cylinder placed upstream of a NACA 0012 airfoil. This simplified flow configuration, well-known in the literature as rod-airfoil problem, allows a parametric study of noise sources from the airfoil leading edge.

The problem involving an airfoil immersed in a cylinder vortex wake was first investigated by Casalino *et al.* (2003), who proposed this simplified model to investigate the sources of leading edge noise of an airfoil. Their analysis was carried out using a hybrid method consisting of a compressible unsteady Reynolds-averaged Navier-Stokes formulation, URANS, with the Ffowcs Williams and Hawkings, FWH acoustic analogy. The methodology was implemented using a 2-D structured mesh to reduce the computational cost of the simulations and three-dimensional effects on far-field noise were modeled by a statistical model. The flow configuration comprised a cylinder with diameter $D = 0.16c$, with c as the airfoil chord, and the distance between the center of the cylinder and the airfoil leading edge, LE, was set as $b = 1.12c$. The Reynolds number based on the airfoil chord was $Re_c = 1.37 \times 10^5$ and the Reynolds number based on the cylinder diameter was $Re_D = 2.2 \times 10^4$. It was shown that the airfoil contribution to far field noise was dominant and provided a good estimate of the overall noise from the whole configuration. Since the method adopted had a series of simplifications, results showed an over prediction of the shedding frequency by 25% and the broadband component of the wall-pressure of the rod could not be captured since the turbulent characteristics of the flow were not resolved in the URANS method.

To overcome the limitations from the URANS formulation, other authors have studied the rod-airfoil configuration using hybrid methods consisting of large eddy simulation, LES, (Giret *et al.*, 2012) and detached eddy simulation, DES, (Greschner *et al.*, 2008). These studies considered moderate Reynolds numbers similar to that from the work by Casalino *et al.* (2003). In both references, the FWH equation was used for far-field noise radiation. The previous authors employed such unsteady formulations with aiming to capture the broadband component of the wall-pressure spectra of the rod. Recently, Giret and Sengissen (2015) performed an LES calculation for a cylinder with $D = 0.1c$ positioned $1.0c$ of distance to the airfoil leading edge. It was shown that the vortex-shedding frequency emissions of the rod-airfoil configuration mostly contribute to the OASPL, except at grazing angles of the observers, where the first harmonic contribution dominates and the tonal peak does not appear in the noise predictions.

Eltaweel and Wang (2012) applied LES together with a boundary element method, BEM, to study the rod-airfoil problem. They showed that, for a fixed cylinder diameter, the airfoil is the dominant source of sound for the lower frequencies while the cylinder becomes important to the overall sound pressure level, OASPL, as the frequency gets higher. The analysis of the separate contributions in terms of leading edge and trailing edge, TE, noise was conducted for the cases investigated and the authors showed that the LE was dominant for the lower frequencies analyzed, and the trailing edge became important as the frequency increased, having the same importance, or even higher, than the leading edge to the total noise radiation. In the same work, the authors showed that the total far-field sound was dominated by the airfoil-wake interaction with the rod contributing almost equally to the shedding peak at positions away from the normal direction measured from the cylinder.

An experimental study was performed by Giesler and Sarradj (2009) to investigate the broadband noise generated from a rod-airfoil configuration. It was shown that the variation of some flow parameters, such as the airfoil thickness, the cylinder diameter and the gap between the cylinder and the airfoil LE considerably impacted the total noise radiation. The authors stated that the leading edge noise was higher than the TE noise for all cases analyzed, and its strength depended on the thickness of the airfoil. On this matter, it was shown that for a thin airfoil such as the NACA0012, the disparity between the TE and LE noise was much higher than that for a thicker airfoil, for instance the NACA0018. In the same work, the authors also concluded, based on experimental observations, that, in general, the LE noise became lower as the cylinder diameter was increased. They argued that a possible cause for this observation could be the lower flow velocities in the wake of the larger cylinders. Finally, the authors compared the results obtained for different gaps among the geometries tested and they concluded that both the LE and TE noise were more dependent on the rod diameter than on the gap between rod and airfoil.

This work presents a detailed analysis of the physical mechanisms responsible for noise generation in a rod-airfoil configuration. We perform 2-D direct numerical simulations, DNS, for laminar flows in order to investigate the tonal noise generation from the cylinder wake. One should remind that, even for turbulent flows with higher Reynolds numbers, a tonal component may be present in the far-field noise spectrum due to coherent structures appearing in the cylinder wake. Moreover, the dominant source of sound for the rod-airfoil configurations available in the literature is due to cylinder vortex shedding, responsible for a tonal peak which is essentially a 2-D physical mechanism. The simplified problem investigated allows us to conduct a detailed parametric study of the LE sources of sound. One should mention that, in this problem, there will be other sources of sound, for example, the noise generated by the non-stationary forces over the surface of the cylinder and the airfoil trailing edge, beyond the quadrupole sources present in the aerodynamic wakes. Here, we investigate the effects of flow compressibility, cylinder-airfoil gap and the ratio between the cylinder diameter and the airfoil chord. In order to assess the accuracy of the numerical solutions, direct noise calculations from the DNS are compared to far-field predictions obtained by the FWH acoustic analogy formulation. The use of the FWH equation also allows one to investigate the separate contributions from the cylinder and airfoil surface sources.

2. FLOW SIMULATIONS

In the present flow simulations, the general curvilinear form of the compressible Navier-Stokes equations is solved in conservation form. The numerical scheme for spatial discretization is a sixth-order accurate compact scheme (Nagarajan *et al.*, 2003) implemented on a staggered grid. The current numerical capability allows the use of overset grids with a fourth-order accurate Hermite interpolation between grid blocks (Bhaskaran and Lele, 2010). Compact finite-difference schemes are non-dissipative and numerical instabilities arising from mesh non-uniformities and interpolation at grid interfaces have to be filtered to preserve stability of the numerical schemes. The high wavenumber compact filter presented by Lele (1992) is applied to the computed solution at prescribed time intervals in order to control numerical instabilities. This filter is only applied in flow regions outside of boundary layers.

The time integration of the fluid equations is carried out by the fully implicit second-order scheme of Beam and Warming (Beam and Warming, 1978) in the near-wall region in order to overcome the time step restriction due to the usual near-wall fine-grid numerical stiffness. A third-order Runge-Kutta scheme is used for time advancement of the equations in flow regions far away from solid boundaries. No-slip adiabatic wall boundary conditions are applied along the solid surfaces and characteristic plus sponge boundary conditions are applied in the far field locations. The numerical tool has been previously validated for several simulations of compressible flows involving sound generation and propagation (Wolf and Lele, 2010; Wolf *et al.*, 2012). Calculations are performed using non-dimensional quantities, using the freestream density, temperature and speed of sound as reference quantities, and the airfoil chord as reference length.

3. ACOUSTIC PREDICTIONS

The FWH acoustic analogy formulation is used to predict the acoustic field radiated by the unsteady flow simulations. The frequency domain FWH equation in integral form is written, as suggested by Lockard (2000), as

$$\left[\hat{p}'H(f)\right] = -\int_{f=0}\left[i\omega\hat{Q}(\vec{y})G(\vec{x},\vec{y}) + \hat{F}_i(\vec{y})\frac{\partial G(\vec{x},\vec{y})}{\partial y_i}\right]dS - \int_{f>0}\hat{T}_{ij}H(f)\frac{\partial^2 G(\vec{x},\vec{y})}{\partial y_i \partial y_j}dV, \quad (1)$$

where p' is the acoustic pressure, ω is the angular frequency, $\vec{y}$ is a source location, $\vec{x}$ is an observer location and the term $\hat{\cdot}$ represents a Fourier transformed quantity. The monopole and dipole source terms are

$$Q = \left[\rho\left(u_i + U_i\right) - \rho_0 U_i\right]\partial f/\partial x_i \quad (2)$$

and

$$F_i = \left[p\delta_{ij} - \tau_{ij} + \rho\left(u_i - U_i\right)\left(u_j + U_j\right) + \rho_0 U_i U_j\right]\partial f/\partial x_j, \quad (3)$$

respectively, and T_{ij} is the Lighthill stress tensor or quadrupole source term given by

$$T_{ij} = \rho u_i u_j + (p' - a^2\rho')\delta_{ij} - \tau_{ij}. \quad (4)$$

In Eqs. 2, 3 and 4, u_i is the fluid velocity vector, U_i is the FW-H surface velocity, p is the pressure, ρ_0 is the freestream density, ρ' and p' stand for the density and pressure perturbations, respectively, a is the speed of sound, δ_{ij} is the Kronecker delta and τ_{ij} is the viscous stress tensor. The term $f = 0$ represents the FW-H surface and $H(f)$ is the Heaviside function defined as $H(f) = 1$ for $f > 0$ and $H(f) = 0$ for $f < 0$. Source terms, observer locations and scattering bodies are assumed to be in steady uniform motion with $\vec{U} = (-U_1, 0)^t$. Therefore, the FW-H surface velocity and the mean convection speed in the observer region are equivalent. In summary, the present work assumes that the airfoil, cylinder and observers are stationary, and there is a uniform flow of speed U_i. The convective Green's function is given by

$$G(\vec{x},\vec{y}) = \frac{i}{4\sqrt{1-M^2}}e^{iM\frac{k}{(1-M^2)}(x_1-y_1)}H_0^{(2)}\left(\frac{k}{(1-M^2)}\sqrt{(x_1-y_1)^2 + (1-M^2)(x_2-y_2)^2}\right), \quad (5)$$

where M is the freestream Mach number defined as $M \equiv U_1/a$, k is the acoustic wavenumber and $H_0^{(2)}$ is the Hankel function of the second kind and order zero.

In the present work, the surface integrations appearing in Eq. 1 are computed along the scattering body surfaces. Therefore, $u_i = -U_i$ for the monopole and dipole source terms, which are then given by $Q = -\rho_0 U_i \partial f/\partial y_i$ and $F_i = \left[p\delta_{ij} + \rho_0 U_i U_j\right]\partial f/\partial y_j$, respectively. Furthermore, one can observe that the monopole source terms, Q, and the second component of the dipole source terms, $\rho_0 U_i U_j$, are steady in time and do not appear in the frequency domain formulation. With the present numerical formulation, it is possible to investigate the individual contributions of the surface dipole sources from the airfoil and from the cylinder. Hence, one can analyze the specific contributions from each of these terms to the total noise generation for a particular frequency.

4. RESULTS

Flow simulations are performed in order to understand the effects of different parameters in the rod-airfoil configuration to the far-field noise radiation. These parameters include the ratio between the cylinder diameter and the airfoil chord, the gap between the cylinder and the airfoil leading edge and the freestream Mach number, M_∞. The meshes used in the simulations are presented in Figs. 1 (a) and (b), being respectively the background mesh, which is Cartesian, and the cylinder and airfoil meshes, which conform to the body. The background mesh has a gentle stretching and contains 1000×640 points in the ξ and η directions, respectively. This mesh is designed to accurately capture the sound waves generated by the rod-airfoil configuration. The cylinder and airfoil meshes have 320×121 and 400×101 points, respectively, and are designed to resolve the boundary layers. For all conforming meshes, ξ and η are the tangential and normal directions to the geometries.

For the problems investigated, the Reynolds number based on the airfoil chord is $Re_c = 5000$. The Reynolds numbers based on the cylinder diameters are $Re_D = 500$ for $D = 0.1c$, and $Re_D = 1000$ for $D = 0.2c$. The Mach numbers investigated here are $M_\infty = 0.1$ and $M_\infty = 0.3$. Figures 2 (a) and (b) show the contours of z-vorticity for $M_\infty = 0.1$ and 0.3, respectively, for a cylinder with $D = 0.1c$. One can notice from these figures that the vorticity intensity is lower for $M_\infty = 0.1$ and the interaction between the vortical structures is much stronger for the higher Mach number, specially at the trailing edge region. For the lower Mach number case, the vortical structures are advected past the trailing edge without any contact to the TE surface, whereas, for $M_\infty = 0.3$, the TE region is dominated by a strong interaction between the vortices coming from both sides of the airfoil.

Contours of dilatation for $M_\infty = 0.1$ and 0.3 are shown in Figs. 3 (a) and (b), for the same case discussed above. It can be inferred from these acoustics fields that the wave number is lower for $M_\infty = 0.1$ and the acoustic radiation patterns

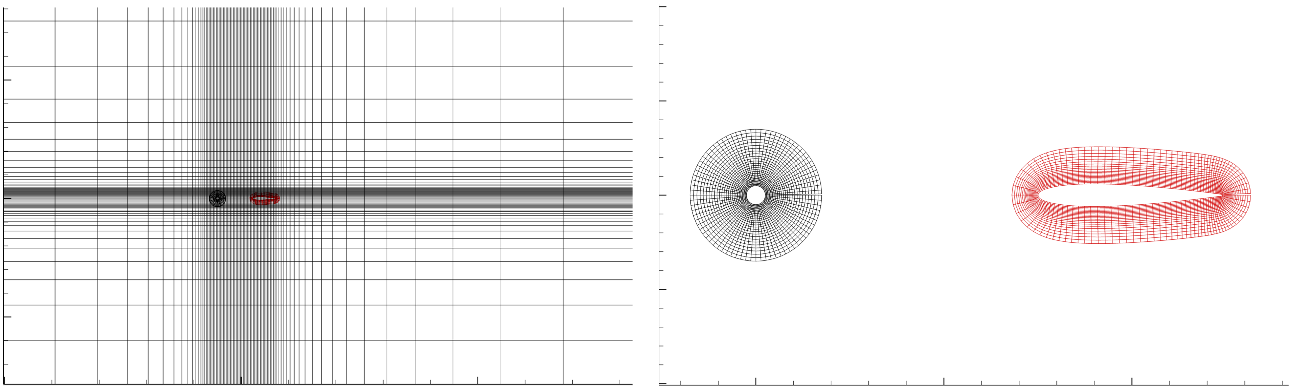

(a) Background mesh with 12 points skip in directions ξ and η. (b) Rod-airfoil meshes with 4 points skip in directions ξ and η.

Figure 1. Mesh configurations used in the test cases analyzed.

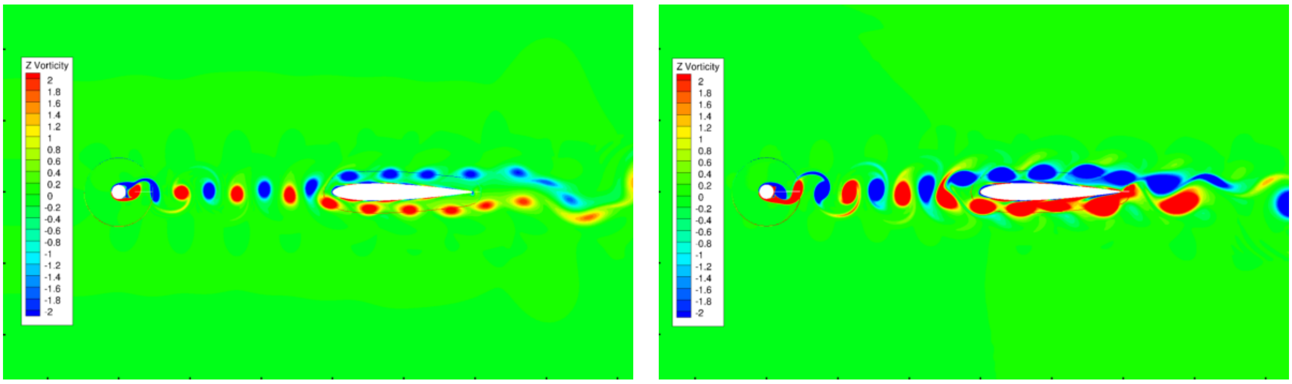

(a) $M_\infty = 0.1$. (b) $M_\infty = 0.3$.

Figure 2. Contours of z-vorticity for the cylinder positioned $-1.5c$ upstream the airfoil leading edge with diameter of $0.1c$.

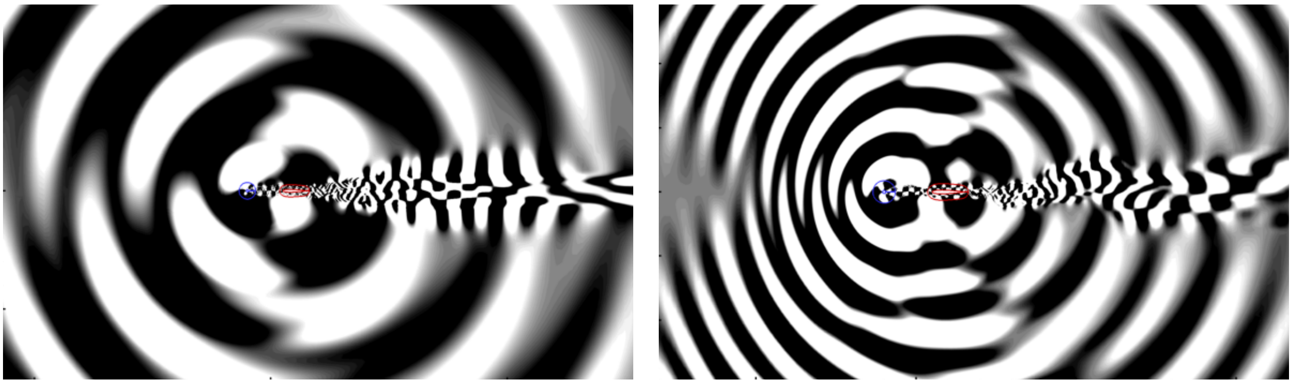

(a) $M_\infty = 0.1$. (b) $M_\infty = 0.3$.

Figure 3. Contours of dilatation for the cylinder positioned at $-1.5c$ upstream the airfoil leading edge with diameter of $0.1c$.

differs from one another. The directivities of pressure fluctuation, $p^{'}$, obtained for the contours of dilatation just discussed are shown in Figs. 4 (a) and (b), where the cylinder and the airfoil dipoles are plotted separately. For $M_\infty = 0.1$, one can notice the similarity, in terms of pressure fluctuation intensity, between the two dipoles, with a small dominance of the airfoil dipole in the far-field noise radiation compared to the cylinder dipole. This configuration presents a low frequency pattern for the dipole directivities as discussed by Curle (1955).

For $M_\infty = 0.3$, the directivity pattern for the cylinder is still similar to that for $M_\infty = 0.1$ since the cylinder is a compact source. However, the airfoil directivity starts to resemble that of a cardioid expected for a trailing edge at higher frequencies. However, here the noise is generated at the leading edge of the airfoil due to the incident vortical structure. Therefore, the direction of the radiation is downstream, differently from the typical TE noise. This fact shows the existence of a similarity between the TE and LE noise radiation; for TE noise, the sources of pressure fluctuations

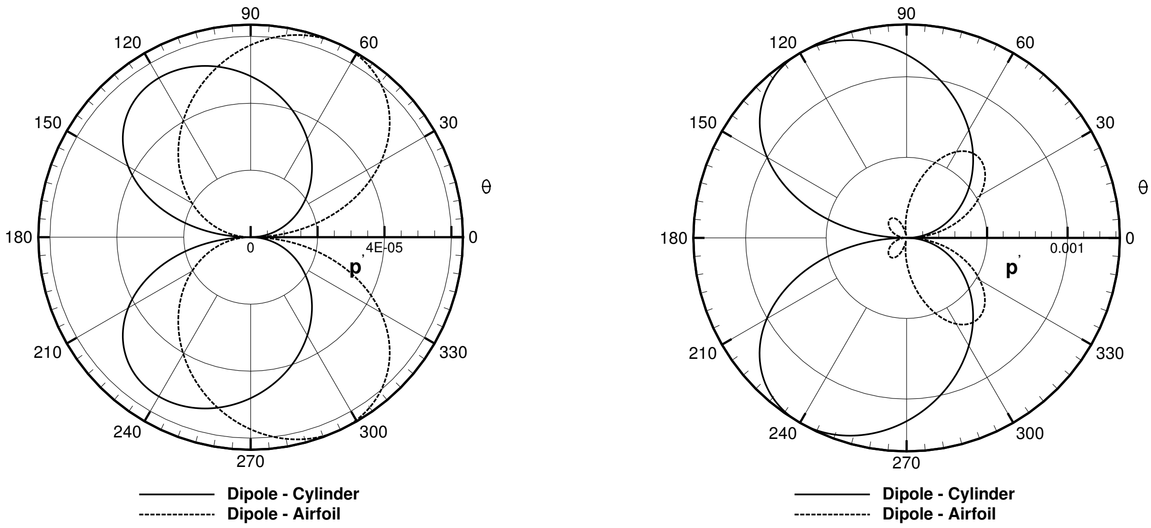

(a) $M_\infty = 0.1$. (b) $M_\infty = 0.3$.

Figure 4. Dipole directivities of separate sources for the cylinder with diameter of $0.1c$ positioned at $-1.5c$ upstream the airfoil leading edge.

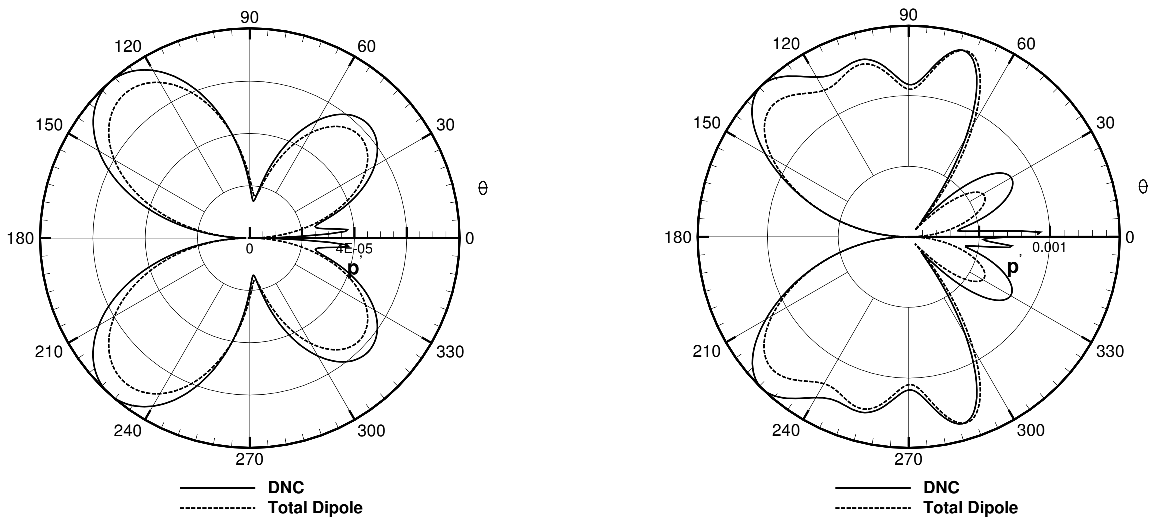

(a) $M_\infty = 0.1$. (b) $M_\infty = 0.3$.

Figure 5. Total dipole directivities and total far-field noise for the cylinder with diameter of $0.1c$ positioned at $-1.5c$ upstream the airfoil leading edge.

along the airfoil are due to vortical structures that interact with the TE surface while for the rod-airfoil problem, LE noise appears due to the vortices impinging on the LE of the airfoil.

Figures 5 (a) and (b) show the total directivities for the Mach numbers investigated. In these plots one can see a good agreement between the FW-H and the DNC (Direct Noise Calculation) obtained directly from the DNS results through a transformation from the time domain to the frequency domain. The quadrupolar directivity encountered in Fig. 5(a) is a result of the phase opposition between the cylinder and airfoil compact dipoles, which are placed in proximity to each other. For $M_\infty = 0.3$, the total noise directivity has a more complex shape. Here, the cylinder vortex-shedding is the dominant source of sound compared to the airfoil. Comparing Figs. (a) and (b), one can see the large impact due to the Mach number variation; not only the shape of the total directivities are modified but the amplitude of pressure fluctuation increases by one order of magnitude as the Mach number goes from $M_\infty = 0.1$ to $M_\infty = 0.3$.

The analysis for the larger cylinder with $D = 0.2c$ is conducted to identify the effects of changing the vortex length compared to the thickness of the leading edge (and the airfoil). Results are compared to those previously obtained for $D = 0.1c$ and the contours of z-vorticity for $M_\infty = 0.1$ and 0.3 are presented in Figs. 6 (a) and (b). One can notice from these figures that there are 2 vortex-shedding periods between the cylinder and the airfoil, while for the $D = 0.1c$ cylinder case, there are 4 periods. Since the cylinder has doubled its size, and the Strouhal number for a cylinder at the present Reynolds number is $St = fD/c \approx 0.2$, the shedding frequency for the $D = 0.1c$ must be twice that for $D = 0.2c$. For the present cases with larger cylinder diameter, the vortices impinge directly on the leading edge surface, breaking up their structure and splitting along both sides of the airfoil. This causes a strong vortex-surface interaction for both Mach numbers, differently from the smaller cylinder case, in which the vortices were convected upward and downward the airfoil without having any direct contact with the LE surface. From the same figures, one can notice that the interaction between the vortex structures occurs for both Mach numbers, with a stronger intensity for $M_\infty = 0.3$, specially on the LE region. At the trailing edge region, the flow-structure interaction is stronger for the higher Mach number case since there is a strong mixing of vortices. The same behavior is observed for the case with a smaller cylinder.

Figures 7 (a) and (b) show the contours of dilatation for the cylinder with $D = 0.2c$. In these snapshots, one can infer that the frequency for $M_\infty = 0.3$ is higher than that observed for $M_\infty = 0.1$. Comparing the dipole directivities of the airfoil and cylinder separately, in Figs. 8 (a) and(b), we can notice the similar behavior of the dipole directivities for both Mach numbers. For the present case, the airfoil dipole radiation is dominant in the far-field. Its amplitude is increased by a factor of ≈ 10 as the flow velocity gets higher and the difference in amplitude between the airfoil and the cylinder dipoles does not change significantly. The total directivities are shown in Figs 9 (a) and (b) and present a good agreement between the results obtained for the FW-H analogy and those from DNC. One can see from these total directivities that, while the separate dipoles have a similar pattern, the total radiation does not. Here, the higher frequency case for $M_\infty = 0.3$ presents a total noise radiation similar to a "bean" shape, with a stronger radiation towards the LE region. Comparing the results obtained for both cylinder sizes, one can imply that the far-field noise radiation has a stronger intensity for the larger cylinder and the directivity patterns are also modified as the shedding frequency is changed.

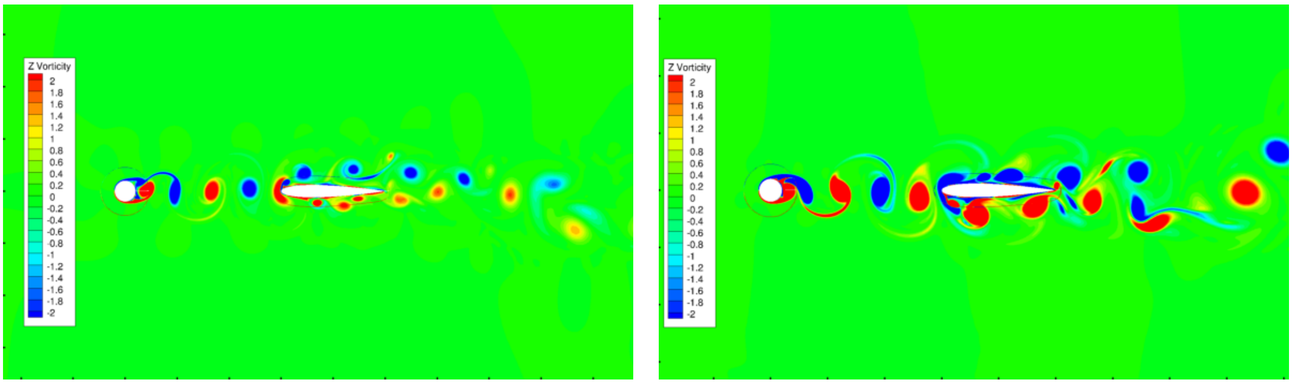

(a) $M_\infty = 0.1$. (b) $M_\infty = 0.3$.

Figure 6. Contours of z-vorticity for the cylinder with diameter of $0.2c$ positioned $-1.5c$ upstream the airfoil leading edge.

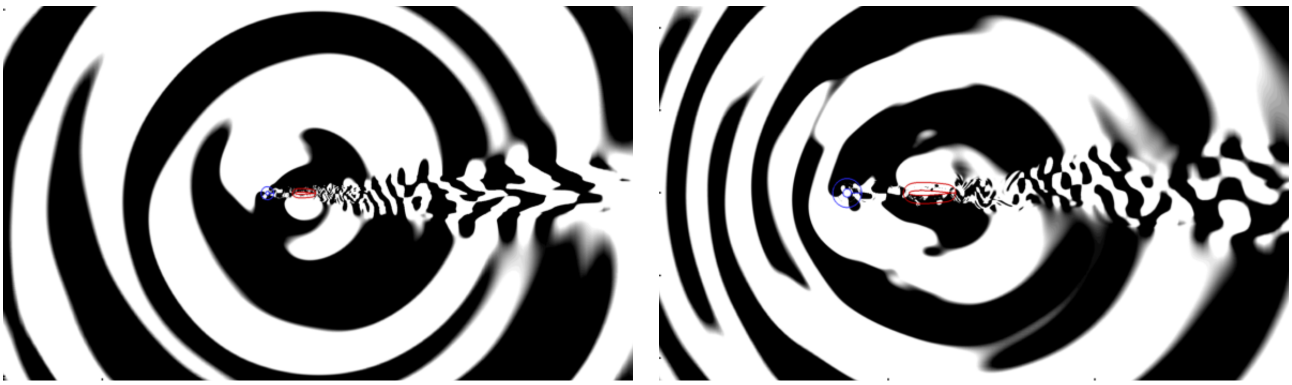

(a) $M_\infty = 0.1$. (b) $M_\infty = 0.3$.

Figure 7. Contours of dilatation for the cylinder with diameter of $0.2c$ positioned at $-1.5c$ upstream the airfoil leading edge.

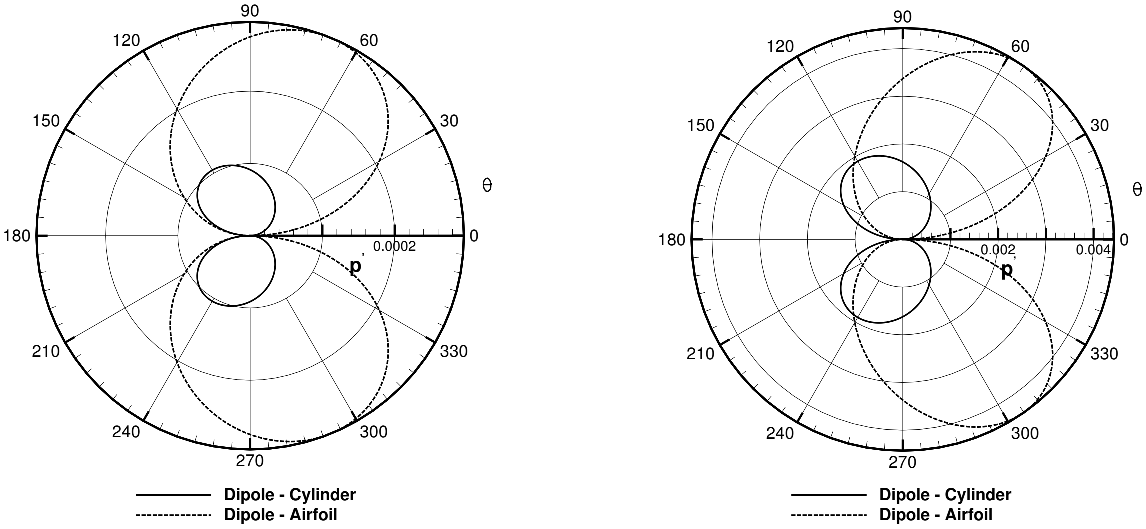

(a) $M_\infty = 0.1$. (b) $M_\infty = 0.3$.

Figure 8. Dipole directivities of separate sources for the cylinder with diameter of $0.2c$ positioned at $-1.5c$ upstream the airfoil leading edge.

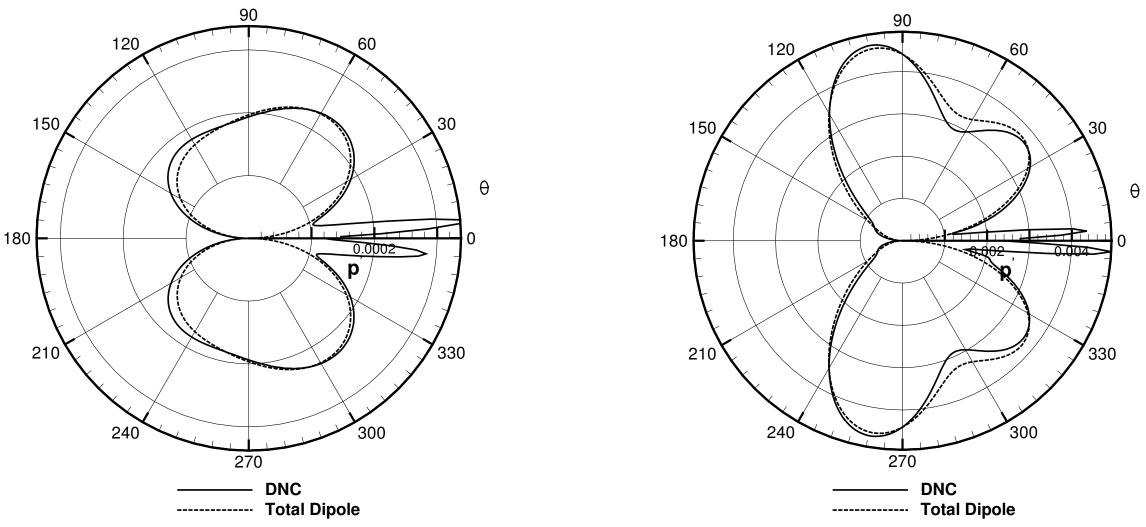

(a) $M_\infty = 0.1$. (b) $M_\infty = 0.3$.

Figure 9. Total dipole directivities and total far-field noise for the cylinder with diameter of $0.2c$ positioned at $-1.5c$ upstream the airfoil leading edge.

5. CONCLUSIONS

A parametric analysis of a rod-airfoil configuration was conducted in order to predict the dependency of the noise radiation on the wave length and the flow compressibility.

For the cases investigated it was possible to notice that for a cylinder with $D = 0.1c$, the increasing of the Mach number, makes the cylinder to be a main source of sound, whereas for $M_\infty = 0.1$ the airfoil has that dominance to the farfield noise radiation. The airfoil has a loss of importance to the total noise radiation as the Mach number gets higher. For $D = 0.2c$, it was possible to see the importance of the airfoil dipole to the total noise radiation for this diameter regardless the Mach number investigated. In terms of noise intensity, one could conclude that the pressure fluctuation is stronger for the bigger cylinder.

A detailed analysis of the LE/TE separate contribution to the farfield noise radiation will be conducted in the future, in order to estimate the factors that influence the most the TE noise generation.

6. ACKNOWLEDGEMENTS

The authors acknowledge the financial support received from Fundação de Amparo á Pesquisa do Estado de São Paulo, FAPESP, under Grant No. 2013/03413-4 and from Conselho Nacional de Desenvolvimento Científico e Tecnológico CNPq, under Grant No. 470695/2013-7. The authors also ackonwledge the FAEPEX M.Sc. fellowship provided by Pró-Reitoria de Pesquisa of University of Campinas, PRP-UNICAMP. The computational resources provided by CENAPAD-SP under Project No. 551 are also acknowledged.

7. REFERENCES

Beam, R.M. and Warming, R.F., 1978. "An implicit factored scheme for the compressible Navier-Stokes equations". *AIAA Journal*, Vol. 16, No. 4, pp. 393–402.

Bhaskaran, R. and Lele, S.K., 2010. "Large eddy simulation of free-stream turbulence effects on heat transfer to a high-pressure turbine cascade". *Journal of Turbulence*, Vol. 11, No. 11, pp. 1–15.

Casalino, D., Jacob, M.C., and Roger, M., 2003. "Prediction of rod-airfoil interaction noise using the ffowcs-williams and hawkings analogy." *AIAA Journal*, Vol. 41, No. 2, pp. 182–191.

Curle, N., 1955. "The influence of solid boundaries upon aerodynamic sound". *Proceedings of the Royal Society of London. Series A. Mathematical and Physical Sciences*, Vol. 231, No. 1187, pp. 505–514.

Eltaweel, A. and Wang, M., 2012. "Numerical simulation of broadband noise from airfoil-wake interaction". In *AIAA Paper 2011-2802, June 2012*. Proceedings of the 17th AIAA/CEAS Aeroacoustics Conference.

Giesler, J. and Sarradj, E., 2009. "Broadband noise investigation on rod-airfoil configurations". In *Proceedings of Acoustics*. NAG,DAGA.

Giret, J.C., Monreau, S., Boussuge, J.F. and Thiele, F., 2012. "Uncertainty quantification of the far-field noise from a rod-airfoil configuration". In *Proceedings of the Summer Program*. NASA Ames Research Center,CA, pp. 261–270.

Giret, J.C. and Sengissen, A., 2015. "Noise source analysis of a rod-airfoil configuration using unstructured large-eddy simulation." *AIAA Journal*, Vol. to appear.

Greschner, B., Thiele, F., Jacob, M.C. and Casalino, B.J., 2008. "Prediction of sound generated by a rod-airfoil configuration using easm des and the generalised lighthill/fwh analogy." *Journal of Computers and Fluids*, Vol. 37, No. 4, pp. 402–413.

Lele, S.K., 1992. "Compact finite difference schemes with spectral-like resolution". *Journal of Computational Physics*, Vol. 103, No. 1, pp. 16–42.

Lockard, D.P., 2000. "An efficient, two-dimensional implementation of the Ffowcs Williams and Hawkings equation". *Journal of Sound and Vibration*, Vol. 229, pp. 897–911.

Nagarajan, S., Lele, S.K. and Ferziger, J.H., 2003. "A robust high-order compact method for large eddy simulation". *Journal of Computational Physics*, Vol. 191, No. 2, pp. 392–419.

Wolf, W.R., Azevedo, J.L.F. and Lele, S.K., 2012. "Convective effects and the role of quadrupole sources for aerofoil aeroacoustics". *Journal of Fluid Mechanics*, Vol. 708, pp. 502–538.

Wolf, W.R. and Lele, S.K., 2010. "Acoustic analogy formulations accelerated by fast multipole method for two-dimensional aeroacoustic problems". *AIAA Journal*, Vol. 48, pp. 2274–2285.

8. RESPONSIBILITY NOTICE

The authors are the only responsible for the printed material included in this paper.